



HAL
open science

Modelling fluid transfer and slip in a fault zone when integrating heterogeneous hydromechanical characteristics in its internal structure

Frédéric Cappa

► **To cite this version:**

Frédéric Cappa. Modelling fluid transfer and slip in a fault zone when integrating heterogeneous hydromechanical characteristics in its internal structure. *Geophysical Journal International*, 2009, 178 (3), pp.1357-1362. 10.1111/j.1365-246X.2009.04291.x . hal-00411856

HAL Id: hal-00411856

<https://hal.science/hal-00411856>

Submitted on 23 Aug 2021

HAL is a multi-disciplinary open access archive for the deposit and dissemination of scientific research documents, whether they are published or not. The documents may come from teaching and research institutions in France or abroad, or from public or private research centers.

L'archive ouverte pluridisciplinaire **HAL**, est destinée au dépôt et à la diffusion de documents scientifiques de niveau recherche, publiés ou non, émanant des établissements d'enseignement et de recherche français ou étrangers, des laboratoires publics ou privés.



Distributed under a Creative Commons Attribution 4.0 International License

FAST TRACK PAPER

Modelling fluid transfer and slip in a fault zone when integrating heterogeneous hydromechanical characteristics in its internal structure

Frédéric Cappa

GeoAzur (UMR6526), University of Nice Sophia-Antipolis, Côte d'Azur Observatory, 06560 Sophia-Antipolis, France.
E-mail: frederic.cappa@geoazur.unice.fr

Accepted 2009 June 8. Received 2009 June 8; in original form 2009 March 6

SUMMARY

Fluid pressure has significant effects on the mechanical behaviour of fault zones, because it can change dramatically throughout the earthquake cycle. Here, we discuss how the heterogeneity of the fault materials affects the fluid transfer and slip processes in and around a fault zone. We present a numerical analysis of the interaction between fluid, stress and the development of slip in a fault zone with heterogeneous hydromechanical characteristics through the brittle seismogenic portion of the crust. In the model, the fault core, characterized by a low permeability and Young's modulus, is surrounded by a high permeability and more rigid damage zone with spatial variations of the hydromechanical properties. Strain-dependent porosity and permeability equations are specified, and the inelastic response of the material is described by a Coulomb criterion. This study shows various evolutions of fluid overpressure, stress, and slip along the principal shear zone depending on the heterogeneity of the fault. The analysis suggests that a pressure pulse can trigger earthquakes by reducing the effective normal stress of the fault, and that the size of the slip zone and the magnitude of the slip are significantly affected both by the reduction in fault effective strength and by the increase in fault porosity and permeability.

Key words: Geomechanics; Permeability and porosity; Fracture and flow; Fault zone rheology; Earthquake dynamics.

1 INTRODUCTION

The presence of fluids in fault zones of the upper seismogenic crust is evidenced by various types of geological, geophysical and geochemical data and it is widely recognized that these fluids affect earthquake processes, and play an important role at different stages of the seismic cycle (Sibson 1981, 1992a,b, 1994; Rice 1992; Manga & Wang 2007). Progressive increase in fluid pressure is assumed during the interseismic period, from near hydrostatic values after an earthquake to near or above lithostatic values before an earthquake (Sibson 1981, 1992a,b, 1994). Such evolution of fluid pressure in fault zones may play a significant role in the nucleation processes of earthquakes by reducing the effective shear strength, at least locally within the fault. Sources of such high-fluid pressures and pathways of these fluids along fault zones required geodynamic processes such as fluid flow from depth, changes in fault zone porosity and permeability, as well as gouge compaction. Several models have been developed in order to investigate the development of fluid pressures in the upper crust. These models examined the effects of porosity reduction (Walder & Nur 1984), the effects of dilatancy

(Hillers & Miller 2006), the effects of crack sealing (Renard *et al.* 2000), and the effects of contrasted hydromechanical couplings (Cappa *et al.* 2007).

In the brittle portion of the seismogenic crust, fault zones in themselves contain complex structures—generally a fault core and a damage zone—that have distinct mechanical and permeability properties (Vermilye & Scholz 1998; Gudmundsson 1999; Wibberley & Shimamoto 2003; Guglielmi *et al.* 2008). The fault core is a low-permeable zone with small intergranular porosity, whereas the damage zone is a more permeable zone with a macroscopic fracture network. Depending on host rock lithology and fault dimensions and movement, the permeability of the fault zone may vary drastically, making the zone act either as a barrier or as a conduit for fluid flows (Caine *et al.* 1996). Moreover, the permeability of the fault zone changes during slip and the sudden stress reduction associated with earthquakes (Uehara & Shimamoto 2004). Field data and models indicate that the core/damage zone contact often ruptures during earthquakes. Both the core and damage zones grow in thickness with increasing displacement (Vermilye & Scholz 1998), and fractures that open allow fluid flow in those zones. Observations

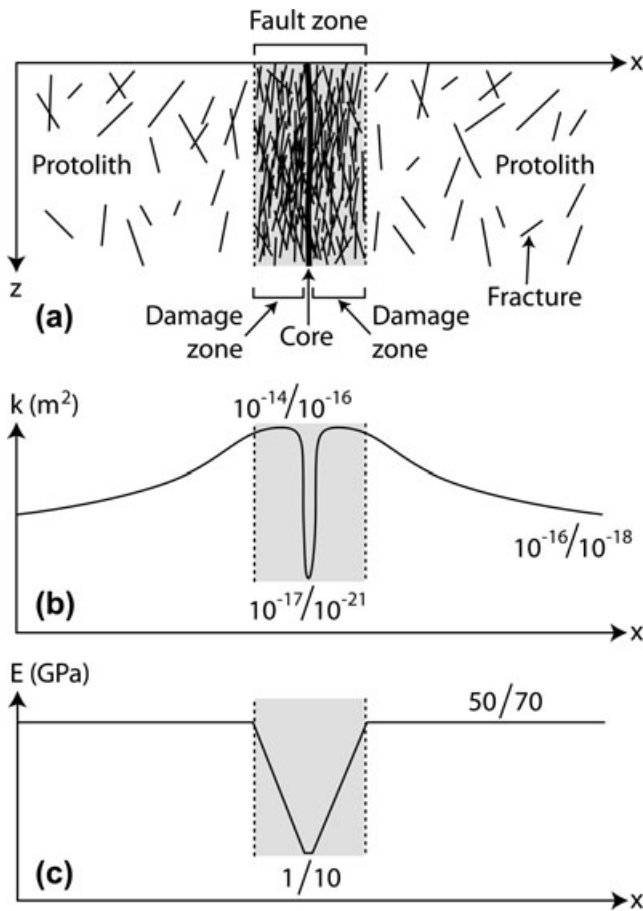


Figure 1. (a) Schematic diagram of the structure across a fault zone and conceptual model of the distribution of (b) permeability and (c) Young's modulus.

of seismic fault zones exhumed from depth or cored by drill holes show that the width of the damage zone is measured at approximately 10 and 50 m on both sides of the central fault plane for common faults (Caine *et al.* 1996; Gudmundsson 2004; Mitchell & Faulkner 2009), and at least several hundreds metres and may be 1–2 km for major fault zones, like the Punchbowl fault on the San Andreas system (Wilson *et al.* 2003) or the Husavik-Flatey fault, a transform fault in North Iceland (Gudmundsson 2007).

The permeability and Young's modulus of fault rock have been measured by several authors (Figs 1a–c, Faulkner & Rutter 2001; Wibberley & Shimamoto 2003; Gudmundsson 2004; Faulkner *et al.* 2006). They found for fault zones in a large variety of country rocks that the permeability of the fault core ranges from 1×10^{-17} to 1×10^{-21} m² (Fig. 1b) and the Young's modulus is measured at approximately 1–10 GPa (Fig. 1c). The areas surrounding the fault core are found to be damaged, intensively fractured and highly permeable. The permeability of this damaged zone is estimated to range from 1×10^{-14} to 1×10^{-16} m²; the Young's modulus is comprised between 10 and 50 GPa (Gudmundsson 2004; Faulkner *et al.* 2006). At the scale of the damage zone, the materials have highly variable properties.

During the seismic cycle, the evolution of the fault zone porosity and permeability may be controlled both by healing and sealing processes, and by the changes in tectonic stresses. The mechanochemical processes tend to decrease the permeability through time by slowly clogging the fault system. An increase in stress can reduce the permeability by closing existing fractures, whereas a decrease

in stress can open the fractures and, then increases the permeability. Thus, permeability enhancement and permeability decrease processes will compete over the seismic cycle and control the fluid flow.

In this paper, we develop a fully coupled thermo-hydro-mechanical model of fluid flow along a vertical fault zone in the upper seismogenic crust using strain-dependent porosity and permeability equations. We consider the effects of hydromechanical characteristics using a heterogeneous distribution of the permeability, the porosity and the Young's modulus in the internal structure of the fault zone as shown in Figs 1(b) and (c). We investigate how this heterogeneity affects the fluid transfer and slip processes in and around the fault zone and how the hydromechanical coupling changes during the inelastic fault response.

2 NUMERICAL MODEL

Let us consider a quasi-static thermohydro-mechanical analysis that assumes a vertical fault zone in a 2-D space (Fig. 2). To investigate the evolution of fluid pressure and slip in the fault zone, we consider a numerical approach, which shows the effect of variable hydromechanical characteristics in the crust and in the fault. The basis of the model is relatively simple. We assumed a lithostatic pressure in a narrow volume around the fault zone at the base of the seismogenic crust. Consequently, the fluid pressure in the fault tends to increase due to the mass transfer from the deep lithostatically overpressured zones to shallow ones at hydrostatic pressure. Potential high-fluid pressure sources at such depths may be initiated by accumulation of seawater, meteoric water, CO₂ degassing or minerals dehydration from the mantle or the lower crust (Manga & Wang 2007). Another alternative for the initiation of such high-fluid pressures can be the coseismic release of fluids trapped at depth (Miller *et al.* 2004). This can occur when earthquake rupturing of low permeability seals release previously trapped high-pressure fluids in reservoirs. Then,

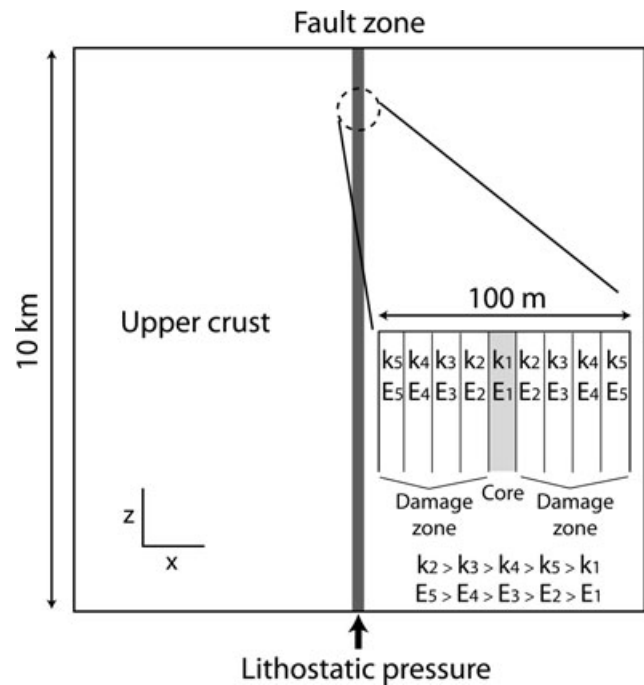


Figure 2. Fault zone model. (inset) Enlargement of fault zone showing the internal structure with the distribution of permeability (k) and Young's modulus (E).

Table 1. Model parameters.

Model parameters	Fault zone Cases 1–2	Fault core Case 3	Fault damage zone Case 3	Crust Cases 1–3
Young's modulus, E (GPa)	10	10	15–50	70
Poisson ratio, ν (–)	0.25	0.25	0.25	0.25
Rock density, ρ_r (kg m^{-3})	2800	2800	2800	2800
Cohesion, c (kPa)	–	–	–	1
Friction coefficient, μ_s	0.6	0.6	0.6	0.75
Dilation angle, ψ ($^\circ$)	20	20	20	–
Zero stress permeability, k_0 (m^2)	1×10^{-16}	1×10^{-19}	1×10^{-14} to 1×10^{-16}	1×10^{-18}
Zero stress porosity, ϕ_0	0.1	0.01	0.02–0.1	0.01
Pore compressibility, β_s (Pa^{-1})	1×10^{-11}	1×10^{-11}	1×10^{-11}	1×10^{-11}
Biot's coefficient, α	1	1	1	1
Thermal expansion, T_e ($1 \text{ }^\circ\text{C}^{-1}$)	1×10^{-6}	1×10^{-6}	8.2×10^{-6}	8.2×10^{-6}
Porosity sensitivity exponent, n	3	3	3	3
Depth sensitivity parameter, β	2600	2600	2600	2600
Fluid density, ρ_f (kg m^{-3})	1000	1000	1000	1000
Fluid viscosity, μ_f (Pa s^{-1})	1×10^{-3}	1×10^{-3}	1×10^{-3}	1×10^{-3}
Fluid compressibility, β_f (Pa^{-1})	2×10^{-10}	2×10^{-10}	2×10^{-10}	2×10^{-10}

large fluxes of fluid can propagate through fault fracture network created during the main shock as pressure pulse.

In the model, fluid flow is simulated using the diffusion equation derived from the continuity of fluid mass and the Darcy's law

$$\nabla \cdot \left[\frac{k}{\mu} (\nabla P - \rho_f g) \right] = S \frac{\partial P}{\partial t}. \quad (1)$$

In this expression, k is the intrinsic permeability, μ is the fluid viscosity, ρ_f is the fluid density, g is the gravity, P is the fluid pressure, t is the time and S is the specific storativity that can be defined in its simplest form as function of the porosity (ϕ), the pore compressibility (β_s), the fluid compressibility (β_f), and the specific weight of fluid (γ)

$$S = \gamma (\beta_s + \phi \beta_f). \quad (2)$$

The appropriate effective stress measure for evaluating strain increments is calculated from the Terzaghi's effective stress (σ'_{ij}) defined as

$$\sigma'_{ij} = \sigma_{ij} - \alpha P \delta_{ij}, \quad (3)$$

where σ_{ij} is the total stress, α is the Biot's coefficient and δ_{ij} is the Kronecker delta.

The model extends vertically to 10 km, and horizontally far enough from the pressurized zone (Fig. 2). Model results are analysed with a special attention to the area near the fault zone, which is distinctly discretized as a 100-m-thick zone with a thin core embedded in a damage zone. The damage zone is composed of multiple, parallel zones, each of which exhibits different hydromechanical characteristics reflecting the heterogeneity of fracture density and properties (Fig. 2). The surrounding crust is considered as much less cracked and with a unique lithology. The numerical grid was refined near the fault zone, with grid sizes gradually increasing towards the lateral model boundaries. The model is fully saturated with water in the liquid phase. Fault zone and crust properties (Table 1) are set consistent with temperature and pressure conditions at depth; in other words, rock physics parameters are defined according to *in situ* stress as well as temperature and pressure conditions. In the model, we assumed that the porosity (ϕ) and the permeability (k) in and around the fault zone change with the total volumetric strain (ε_v) [the sum of the elastic and inelastic ('plastic') components of strain] as follows:

$$\phi = 1 - \left[1 - \left(\phi_0 e^{-\frac{z}{\beta}} \right) \right] e^{-\varepsilon_v} \quad (4)$$

$$k = \left(k_0 e^{-\frac{z}{\beta}} \right) \left(\frac{\phi}{\phi_0 e^{-\frac{z}{\beta}}} \right)^n, \quad (5)$$

where ϕ_0 is the initial porosity at zero stress, z is the depth, β is a depth sensitivity parameter, k_0 is the initial intrinsic permeability at zero stress, n is the porosity sensitivity exponent. In this model, the initial porosity and permeability distribution decreases exponentially with depth. A difference of two orders of magnitude is assumed between the initial values near the ground surface and the ones at the base of the seismogenic crust.

In the simulations, the total volumetric strain is defined as the sum of the elastic ($d\varepsilon^e$) and inelastic ('plastic') ($d\varepsilon^p$) components of strain. We followed Rudnicki & Rice (1975) in formulating the volumetric strain increment during elastoplastic response of dilatant frictional materials. The relationship between stress (τ and σ , shear and compressive components, respectively) and volumetric strain increments is written as:

$$d\varepsilon_v = d\varepsilon^e + d\varepsilon^p = \frac{d\sigma}{K} + \frac{\psi}{h} (d\tau + \mu_s d\sigma), \quad (6)$$

where K and h are the Bulk and plastic hardening moduli, respectively; ψ is the dilatancy factor defined as the ratio of an increment in volumetric plastic strain to an increment in shear plastic strain; and μ_s is the static friction coefficient. During plastic response, the ratio of $(d\tau + \mu_s d\sigma)$ to h is always positive; for hardening both $(d\tau + \mu_s d\sigma)$ and h are positive, for softening both are negative, and for ideally plastic response both vanish such that their limit exists as a positive quantity corresponding to the plastic strain increment. In the simulation results shown here, we considered an ideally plastic response.

In situ and boundary fluid pressures were considered to be hydrostatic. On the top boundary, the ground surface is free to move, whereas stress was set to others boundaries. Temperature is assumed to follow a constant geothermal gradient with depth ($30 \text{ }^\circ\text{C km}^{-1}$). For simplicity, an *in situ* extensional stress regime was assumed with $\sigma_H = 0.75 \sigma_v$.

After computing the initial state, we applied instantaneously a pressurization (i.e. pressure pulse) corresponding to the lithostatic pressure at 10 km depth at the base of the fault zone. In the fault, slip occurs when the shear stress acting in the fault plane exceeds its shear strength, approximated by a Coulomb criterion

$$\tau = c + \mu_s (\sigma_n - \alpha P), \quad (7)$$

where τ is the critical shear stress for slip occurrence, c is cohesion, and σ_n is the normal stress. In the model, we only considered fault slip in the dip direction (i.e. no strike component perpendicular to x - z plane) because of the 2-D geometry.

Consequently, in our model there are two principal types of processes which may change the fluid pressure: (1) the inflow of fluid from depth and (2) the progressive change in porosity and permeability by change in volumetric strain (i.e. dilatancy) in and around the fault zone. Moreover, since the host rock can behave as elastic material, the weight of the rock above the pressure source must be supported by its internal fluid pressure. It follows that the fluid flow is partly driven by buoyancy, due to density difference between the host rock and the fluid. Consequently, the buoyancy effect might increase the fluid overpressure and volumetric flow rate in the fault zone, and thus increase the probability of fault slip.

Three models are compared, one neglecting porosity and permeability changes in a fault zone represented as a unique material (Case 1), one with porosity and permeability changes in a fault zone represented as in case 1 (Case 2) and one with porosity and permeability changes in a fault zone represented as a core and a damage zone with materials of highly contrasted properties (Case 3) as described by the enlargement of the fault zone in Fig. 2. In that case, we assumed a distribution of permeability and Young's mod-

ulus as shown in Figs 1(b) and (c) (see Table 1). Rigorously, the permeability should also vary in the third dimension (i.e. along-strike direction) according to common geological models of fault structure. Within the fault cores, permeability has been shown to vary by several orders of magnitude and can exhibit permeability anisotropy of three orders of magnitude (Faulkner & Rutter 1998). Consequently, permeability in the core can be significantly different in the vertical direction in comparison to the along-strike direction. For simplicity, we will consider that the permeability and porosity in our model will change significantly in the x - z plane during the pressurization. This approximation is the main limit of the model. Indeed, it does not consider the 3-D interaction involved by the geological observations.

We solved the coupled eqs (1)–(6) at each cell using the finite difference method.

3 MODELLING RESULTS

Results indicate that overpressure always develops at the base of the fault due to the inflow of fluid from the source region. All the models show this effect (Figs 3a–d) leading to a localized high-pressure zone. Fluid pressure moves up the fault, escaping from the

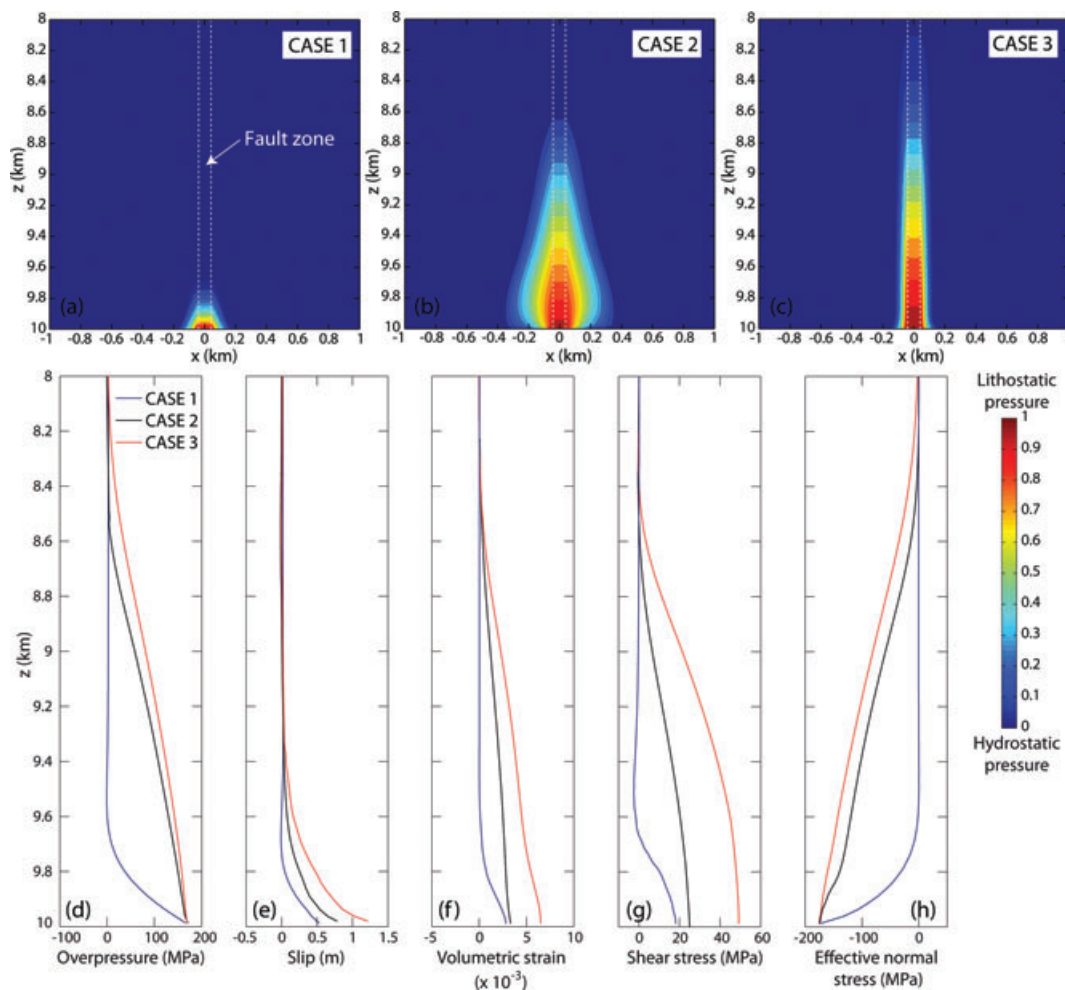


Figure 3. Distribution of fluid overpressure along the fault zone, from hydrostatic (blue) to lithostatic (red) pressure for (a) Case 1, (b) Case 2 and (c) Case 3. Model results when pressure, strain and stress are steady-state: vertical profiles of changes in (d) fluid pressure, (e) slip, (f) volumetric strain, (g) shear stress and (h) effective normal stress along the fault core.

overpressured source region, which produces a pressure gradient that was mainly distributed in the fault zone. Nevertheless, part of the fluid transfer occurs within a large portion of the surrounding crust in Case 2, whereas the fluid pressure slightly increases in the crust very close to fault walls in Cases 1 and 3. Comparing the three cases, results show that change in fluid pressure is highly sensitive to the porosity and permeability change and to the initial porosity and permeability values in the fault zone. Fluid pressure is restricted near the source region when change in permeability and porosity is neglected (Case 1), whereas fluid pressure propagates farther along the fault when porosity and permeability vary with volumetric strain (i.e. dilatational fracture damage variations in and around the damage zone) (Cases 2 and 3). With a fault model represented as a unique material (Case 2), overpressure diffuses upward in the fault along a 1.4-km-long zone and in the crust, about 350 m on each side of the central part of the fault near the source region. With a fault represented as a core and a damage zone with contrasted properties (Case 3), overpressure propagates mainly upward in the fault (i.e. slight lateral diffuse leakage in the crust) along a 1.8-km-long zone because the high permeability damage zone facilitates the flow-through process along the fault and so amplifies the development of overpressure through the fault. Results also show that significantly increased permeability due to fracturing within the damage zone of faults strongly influences fluid flow processes and the extent of the overpressured zone.

Inside the fault core, the overpressure produces a localized weak zone with a lowered effective normal stress, an increased shear stress and an increased volumetric strain resulting in an expansion which is accompanied by an increase in porosity, with a corresponding increase in permeability (Figs 3d–h and 4). The largest variations in stress and strain are obtained for the Case 3 ($\Delta\sigma_n = -175$ MPa; $\Delta\tau = 50$ MPa; $\Delta\varepsilon_v = 7 \times 10^{-3}$). In all cases, this hydromechanical effect induces slip along the fault core. The larger slip is obtained for Case 3 in which slip is about 1.2 m and distributed along a 600 m long active shear zone (Fig. 3e). In Case 1 and 2, slip and shear zone length are lower (by a factor of ~ 2 and ~ 1.5 for Case 1

and Case 2, respectively). In all cases, fault slip occurs progressively during the pressure increase. Results also show that the damage zone deforms inelastically in response to the pressurization and associated localized high stressing near the source region. These inelastic deformations could primarily occur as frictional sliding along pre-existing fractures or microcracking.

Fig. 4 shows that the zone of change in porosity and permeability is larger in Case 2 than in Case 3. In Case 2, porosity and permeability vary in the fault and the surrounding crust with a lateral extent of about 350 m on each side of the central part of the fault near the source region, whereas, in Case 3, the variations are localized in the fault zone. This difference is due to the contrast between the initial values of hydromechanical properties in the two cases. This heterogeneity of the fault induces contrasted fluid, stress and strain transfer in the fault/crust system.

The difference in the three models' behaviour is linked both to the contrast in hydromechanical characteristics among fault zone elements and to the change in fault zone permeability and porosity with volumetric strain. This analysis evidences the effect of the heterogeneity of the initial porosity, permeability and Young's modulus distribution in the damage zone on the hydromechanical behaviour of the fault core (i.e. principal slip zone) where earthquakes can nucleate. In summary, at the scale of the damage zone, the highly variable materials can cause large property variations. The slip process varies along the fault depending on the spatial variations of hydromechanical characteristics and the fluid and stress transfer which reduce the effective fault strength.

4 CONCLUSION

Through a variety of numerical experiments, we have examined the effect of the heterogeneity of the hydromechanical characteristics in a fault zone on the interactions between fluid and stress transfer, enhanced porosity and permeability, and slip dimensions along the principal shear zone of the fault when subjected to high-fluid

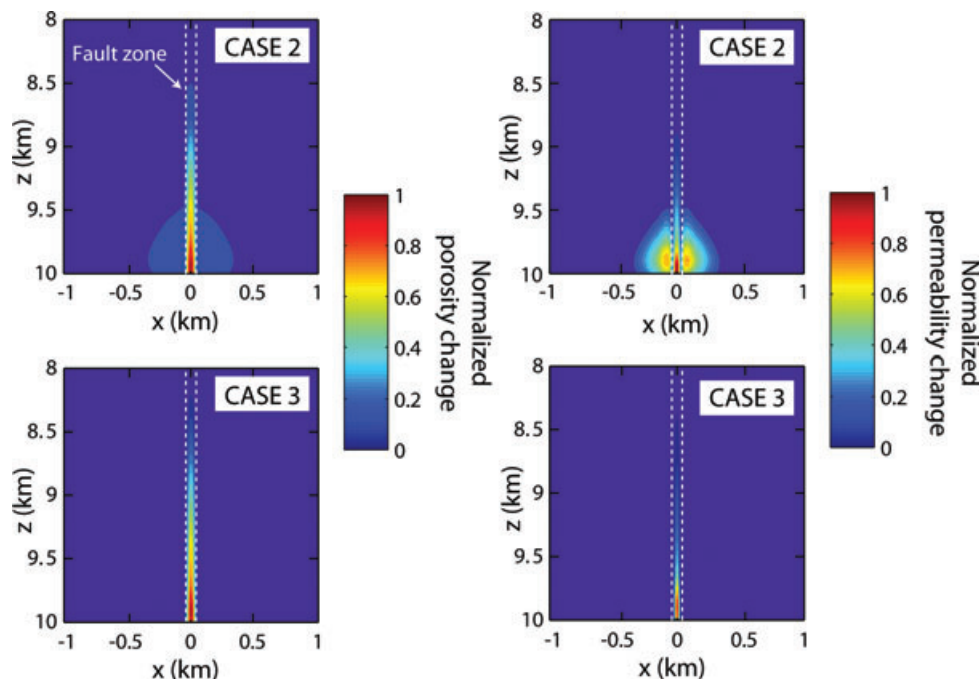


Figure 4. Simulated change in fault zone (normalized) porosity (left-hand panels) and permeability (right-hand panels) for Cases 2 and 3.

pressures diffusing upward through the upper seismogenic crust. Our analysis demonstrated that this heterogeneity of the fault materials significantly affects the location and the evolution of fluid overpressures in the fault zone, and thus the change in its mechanical strength. In the zones of fluid overpressures, the frictional strength is lowered and slip can nucleate along the fault core, and the damage zone can deform inelastically. This study also suggested that the changes in permeability and porosity with volumetric strain mainly control the changes in fluid pressure and flux, and consequently, the rate of hydromechanical processes. Direct observations of such change of fluid pressure, by geophysical or geodetic measurements, above seismically active zones should improve our understanding of earthquakes and the seismic cycle.

In summary, our analysis shows that a pressure pulse can trigger earthquakes by reducing the effective normal stress of the fault, and that the size of the slip zone and the magnitude of the slip are significantly affected by both, the reduction in fault effective strength and the increase in fault porosity and permeability.

Finally, our simple model proves to be promising to analyse the role of fluids in the earthquake mechanisms in crustal-scale fault zones when considering fully hydromechanical couplings. Future improvements of this model could involve the mechano-chemical processes, which also play a significant role during the seismic cycle. Gratier & Gueydan (2007) discussed the importance of these mechano-chemical interactions, within characteristic time intervals, on the weakening and strengthening of faults in the upper crust. Moreover, experimental studies of permeability variations in fresh fractures at seismogenic temperatures have shown permeability can significantly recover over similar timescales of days to weeks (Morrow *et al.* 2001), and microfractures on the order of hours to days (Brantley *et al.* 1990). Consequently, competing fracturing and sealing processes at different scales will control fault zone fluid flow and a variety of geological processes.

ACKNOWLEDGMENTS

I am grateful for the constructive comments and recommendations of the technical reviews by August Gudmundsson and one anonymous reviewer, who helped me to improve my manuscript.

REFERENCES

Brantley, S.L., Evans, B., Hickman, S.H. & Crerar, D.D., 1990. Healing of microcracks in quartz—implications for fluid flow, *Geology*, **18**(2), 136–139.

Caine, J.S., Evans, J.P. & Foster, C.G., 1996. Fault zone architecture and permeability structures, *Geology*, **24**(11), 1025–1028.

Cappa, F., Guglielmi, Y. & Virieux, J., 2007. Stress and fluid transfer in a fault zone due to overpressures in the seismogenic crust, *Geophys. Res. Lett.*, **34**, L05301, doi:10.1029/2006GL028980.

Faulkner, D.R. & Rutter, E.H., 1998. The gas permeability of clay-bearing fault gouge at 20°C, in *Faults, Fault Sealing and Fluid Flow in Hydrocarbon Reservoirs*, pp. 147–156, eds Jones, G., Fisher, Q. & Knipe, R.J., Geol. Soc. Spec. Pub.

Faulkner, D.R. & Rutter, E.H., 2001. Can the maintenance of overpressured fluids in large strike-slip fault zones explain their apparent weakness? *Geology*, **29**, 503–506.

Faulkner, D.R., Mitchell, T.M., Healy, D. & Heap, M., 2006. Slip on ‘weak’ faults by the rotation of regional stress in the fracture damage zone, *Nature*, **444**(7121), 922–925.

Gudmundsson, A., 1999. Fluid overpressure and stress drop in fault zones, *Geophys. Res. Lett.*, **26**(1), 115–118.

Gudmundsson, A., 2004. Effects of Young’s modulus on fault displacement, *CR. Geosci.*, **336**, 85–92.

Gudmundsson, A., 2007. Infrastructure and evolution of ocean-ridge discontinuities in Iceland, *J. Geodyn.*, **43**, 6–29.

Guglielmi, Y., Cappa, F. & Amitrano, D., 2008. High-definition analysis of fluid-induced seismicity related to the mesoscale hydromechanical properties of a fault zone, *Geophys. Res. Lett.*, **35**, L06306, doi:10.1029/2007GL033087.

Gratier, J.P. & Gueydan, F., 2007. Deformation in the presence of fluids and mineral reactions: effect of fracturing and fluid-rocks interaction on seismic cycles, in *The Dynamics of Fault Zones* (95th Dahlem Conference), pp. 319–356, eds Handy, M., Hirth, G., Rice, J., Hovius, N. & Friedrich, A., MIT Press, Cambridge, MA.

Hillers, G. & Miller, S.A., 2006. Dilatancy controlled spatiotemporal slip evolution of a sealed fault with spatial variations of the pore pressure, *Geophys. J. Int.*, **168**, 431–445.

Manga, M. & Wang, C.Y., 2007. Earthquake hydrology, in *Treatise on Geophysics*, Vol. 4, pp. 293–320, ed. Schubert, G. Elsevier, Amsterdam.

Miller, S.A., Collettini, C., Chiaraluce, L., Cocco, M., Barchi, M. & Kaus, B.J.P., 2004. Aftershocks driven by a high-pressure CO₂ source at depth, *Nature*, **427**(6976), 724–727.

Mitchell, T.M. & Faulkner, D.R., 2009. The nature and origin of off-fault damage surrounding strike-slip fault zones with a wide range of displacements: a field study from the Atacama fault system, northern Chile, *J. Struct. Geol.*, doi:10.1016/j.jsg.2009.05.002, in press.

Morrow, C.A., Moore, D.E. & Lockner, D.A., 2001. Permeability reduction in granite under hydrothermal conditions, *J. geophys. Res.*, **106**(B12), 30 551–30 560.

Renard, F., Gratier, J.P. & Jamtveit, B., 2000. Kinetics of crack-sealing, intergranular pressure solution and compaction around active faults, *J. Struct. Geol.*, **22**, 1395–1407.

Rice, J., 1992. Fault stress states, pore pressure distributions, and the weakness of the San Andreas fault, in *Fault Mechanics and Transport Properties in Rocks*, pp. 475–503, eds Evans, B. & Wong, T.F., Academic Press, San Diego, California.

Rudnicki, J.W. & Rice, J.R., 1975. Conditions for localization of deformation in pressure-sensitive dilatant materials, *J. Mech. Phys. Solids*, **23**, 371–394.

Sibson, R.H., 1981. Fluid flow accompanying faulting: Field evidence and models, in *Earthquake Prediction: An International Review*, Maurice Ewing Ser., 4, pp. 593–603, eds Simpson, D.W. & Richards, P.G., AGU, Washington, DC.

Sibson, R.H., 1992a. Fault-valve behavior and the hydrostatic-lithostatic fluid pressure interface, *Earth-Sci. Rev., Metamorphic Fluids*, **32**(1–2), 141–144.

Sibson, R.H., 1992b. Implications of fault-valve behavior for rupture nucleation and recurrence, *Tectonophysics*, **211**, 283–293.

Sibson, R.H., 1994. Crustal stress, faulting and fluid flow, *Geol. Soc., Lond., Special Publ.*, **78**, 69–84.

Uehara, S.I. & Shimamoto, T., 2004. Gas permeability evolution of cataclastic and fault gouge in triaxial compression and implications for changes in fault-zone permeability structure through the earthquake cycle, *Tectonophysics*, **378**, 183–195.

Vermilye, J.M. & Scholz, C.H., 1998. The process zone: a microstructural view of fault growth, *J. geophys. Res.*, **103**(B6), 12 223–12 237.

Walder, J. & Nur, A., 1984. Porosity reduction and crustal pore pressure development, *J. geophys. Res.*, **89**, 11 539–11 548.

Wibberley, C.A.J. & Shimamoto, T., 2003. Internal structure and permeability of a major strike-slip fault zones: the median tectonic line in Mie prefecture, Southwest Japan, *J. Struct. Geol.*, **25**, 59–78.

Wilson, J.E., Chester, J.S. & Chester, F.M., 2003. Microfracture analysis of fault growth and wear processes, Punchbowl Fault, San Andreas System, California, *J. Struct. Geol.*, **25**(11), 1855–1873.